Schweizerischer Erdbebendienst
Service Sismologique Suisse
Servizio Sismico Svizzero
Swiss Seismological Service

ETH zürich

SITE CHARACTERIZATION REPORT

SWIK: Wil (SG) - Kantonsschule

Clotaire Michel, Manuel Hobiger, Donat Fäh

Last Modification: 1st December, 2016

Schweizerischer Erdbebendienst (SED)
Service Sismologique Suisse
Servizio Sismico Svizzero
Servizi da Terratrembels Svizzer

ETH Zurich
Sonneggstrasse 5
8092 Zurich
Schweiz
clotaire@sed.ethz.ch

Contents

Summary

The new station SWIK was installed in the secondary school area in Wil (SG) and the installation site has been characterized. We performed passive seismic array measurements that successfully allowed us to retrieve 1D velocity profiles at the station site. The site is perfectly 1D and could be used as benchmark for future studies. The profiles show 90 m of alluvial and lacustrine sediments with velocities from 400 to 750 m/s. A clear contrast within the sediments is present at 40 m depth. A possible zone of higher velocities ranges from 1 to 6 m depth without definitive justification. The velocity contrast is strong with the underlaying Upper Freshwater Molasse (OSM) that is found to be at 1600 m/s.
$V_{s,30}$ is 397 m/s and the site corresponds to ground type B in the Eurocode 8 (CEN, 2004) and type C in the SIA261 (SIA, 2014). The theoretical 1D SH transfer function computed from the inverted profiles shows a large peak at the fundamental frequency at 1.6 Hz reaching an amplification of a factor of 5. This situation is however representative only for the zone around the school area and not for the entire city where higher resonance frequencies and lower velocity contrasts were observed from the H/V measurements.

1 Introduction

In the framework of the second phase of the Swiss Strong Motion Network (SSMNet) renewal project, a new installation in the secondary school in Wil (SG) was decided. It is located in the Thur valley (see Fig. 1) in the Swiss foreland. The new station went operational on 6 October 2015.

Figure 1: Station SWIK in the school area during the array measurement.

2 Geological setting

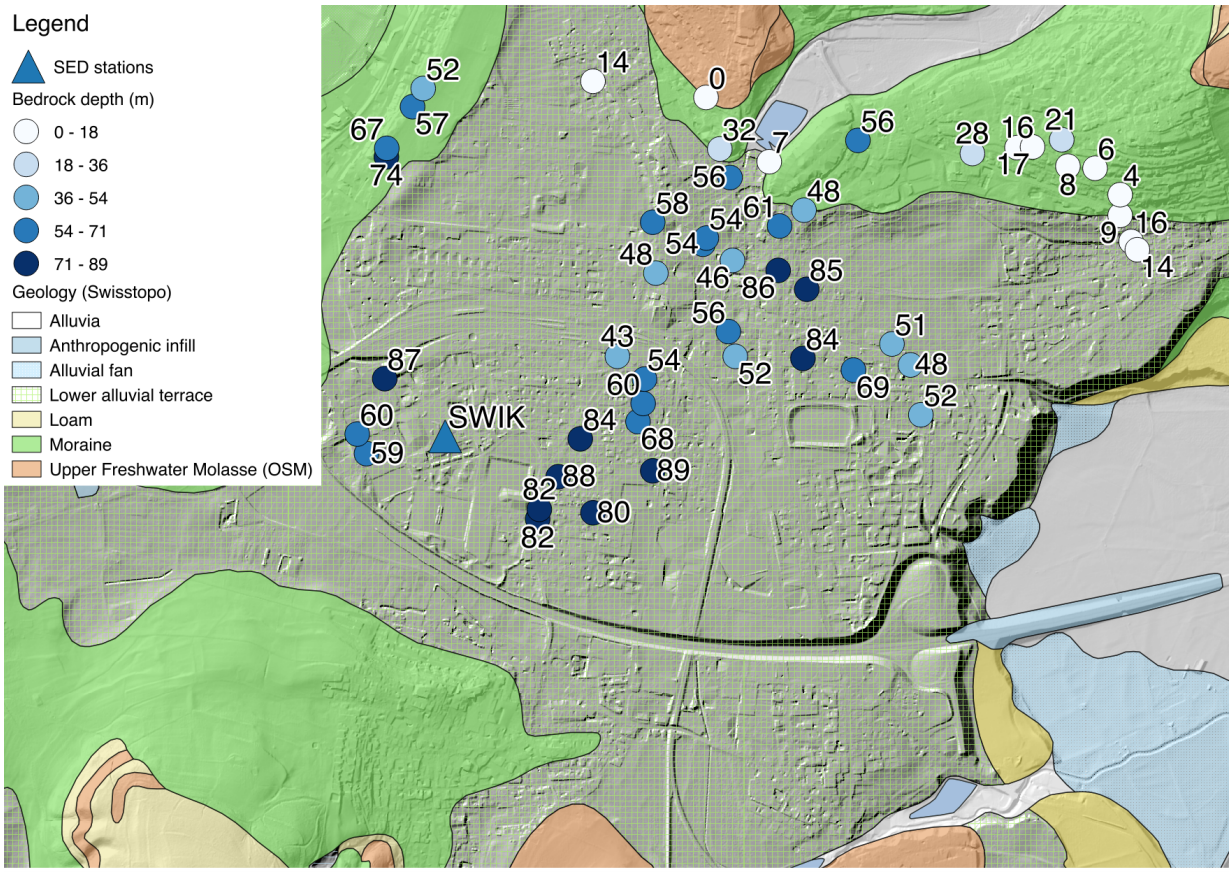

Figure 2: Geological map of the Wil area including the bedrock depth from boreholes superimposed on a relief map (data: © 2016 swisstopo JD100042 and Office for the Environment Kanton St Gallen).

Wil is located in the centre of a small alluvial valley (former flow of the Thur river/glacier) with up to 90 m of Quaternary sediments according to numerous available boreholes of the geoportal of St Gallen administration (`www.geoportal.ch`, Erdwärmesonden KT SG AR AI). Boreholes located close to the school area indicate a thickness of 60 to 90 m of sediments. The sediments are made of lower alluvial terraces (fluvial sediments) according to the geological map (Fig. 2), though the interpretation from some boreholes indicates that the upper layers are made of moraine. About 200 m west from the investigated site, boreholes indicate 32 m of moraine, on top of lacustrine sediments of about the same thickness. At 250 m north of the site, a borehole shows a 15 m thick layer of alluvial sediments on top of 72 m of lacustrine sediments and moraine. Finally, at 350 m to the southwest, the boreholes do not show lacustrine sediments but a 85 m thick layer of post-glacial alluvial and fluvial-glacial sediments, although an interface at about 40 m is noted. No significant amount of water can be noted in the upper layers. The bedrock is made of the Upper Freshwater Molasse (OSM) of Tortonian age (Miocene, Tertiary). The Molasse basin is 2.6 km deep at this location according to the GeoMol project of Swisstopo.

3 Site characterization using passive measurements

3.1 Measurements and data set

We investigated the local underground structure by passive seismic array measurements which took place on October 29th, 2016. The layout of the seismic arrays is shown in Fig. 3. Two configurations were used.
The parameters of both arrays are given in Table 1. For these measurements 12 Nanometrics Centaur dataloggers named NR42 to NR49 and NR52 to NR55 and 14 Lennartz 3C 5 s seismometers were available. Each datalogger can record on 2 ports A (channels EH1, EH2, EH3 for Z, N, E directions) and B (channels EH4, EH5, EH6 for Z, N, E directions). Time synchronization is ensured by GPS. The sensors were placed on metal tripods. For better coupling with the ground, the 10 cm gravel layer in front of the school was removed and the tripods placed on the textile layer located on compacted material below. The sensor coordinates were measured using a differential GPS device (Leica Viva GS10), including only a rover station and using the Real Time Kinematic technique provided by Swisstopo. It allowed an absolute positioning with an accuracy better than 6 cm on the Swissgrid.

Table 1: List of the seismic array measurements in Wil.

Array name	Number of sensors	Minimum interstation distance [m]	Aperture [m]	Recording time [min]
WIK1	14	10	120	123
WIK2	14	10	240	133

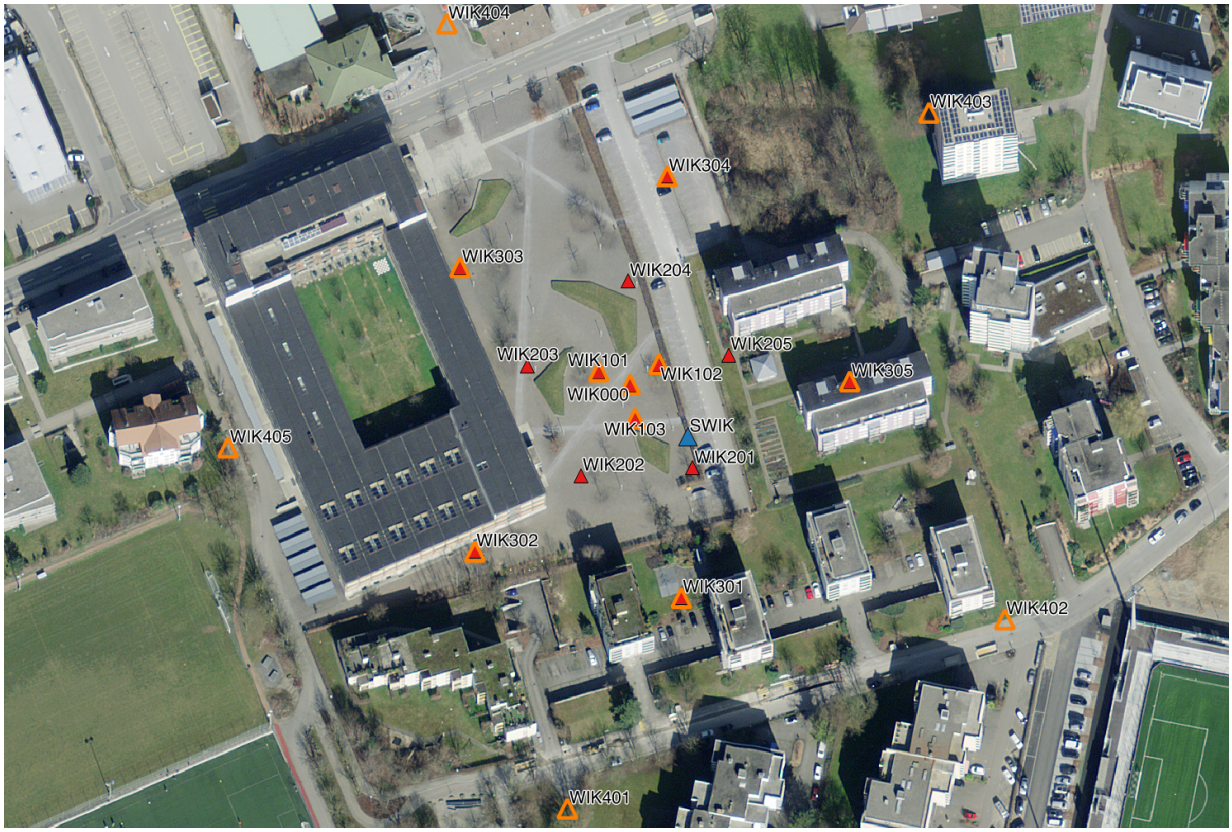

Figure 3: Layout of the array measurements at site SWIK (red: WIK1; orange: WIK2).

The largest time windows were extracted, for which all the sensors of the array were correctly placed and the GPS synchronization was ensured. The recordings are well correlated through the array but many disturbances can be noticed. Especially, a series of strong peaks in the horizontal components from 1.16 to 2.34 Hz can be noticed on all datasets. On the vertical component, a 3.36 Hz peak is very strong, as well as peaks at 6.13, 7.2, 10.14 Hz. Point WIK305 seems to be influenced by the close-by building, with a filtering of the ground motion above 5 Hz. Moreover, WIK403 shows a strong influence of the nearby building, with peaks at 2.5 Hz in the 3 components. This is also the case, with a lower amplitude, for WIK402 (1.93 Hz).
Orientations of the sensors were checked by maximizing the correlation with the central station at low frequencies (Poggi et al., 2012b). Corrections lower than 8 ° were generally observed except at point WIK401 where a correction of 14 ° was necessary.

3.2 Single station measurements results

3.2.1 H/V curves

All H/V curves show the same shape across the array (Fig. 4) that includes a very clear peak at 1.62 Hz with an amplitude of about 5. It shows that the site is 1D. The only slight deviations concern point WIK401 that shows a slightly higher frequency value (1.9 Hz) and point WIK403 that has a different shape of the H/V curve, although with the same peak value. A small peak is observed at 20 Hz on all curves.
No frequency peak can be seen below this fundamental frequency, as confirmed by the H/V ratios computed over 1 week at the two test stations XWIL1 and XWIL2, the latter being located in the school building (Fig. 5). The H/V ratios at XWIL1 are very smooth and it is difficult to pick a fundamental frequency that would be between 2 and 4 Hz, i.e. at higher frequency compared to XWIL1, corresponding therefore to shallower sediments with a weak velocity contrast. According to the available boreholes, the sediment thickness at both sites is not very different (60 to 90 m at XWIL2 and 60 to 70 m at XWIL1). The extreme values of these thickness ranges would however be sufficient to explain the difference in the fundamental frequency. A single station measurement campaign has been conducted in the city and presents the same two types of H/V curves: clear peaks with frequencies lower than 2 Hz close to the investigated site, flatter curves with higher frequency peaks elsewhere. The first type corresponds to a relatively deep feature in the basin (90 m), possibly with softer sediments than in the rest of the city. The correlation between H/V peak and bedrock depth is not obvious for the second type, possibly due to a too low spatial sampling regarding the complexity of the bedrock shape.

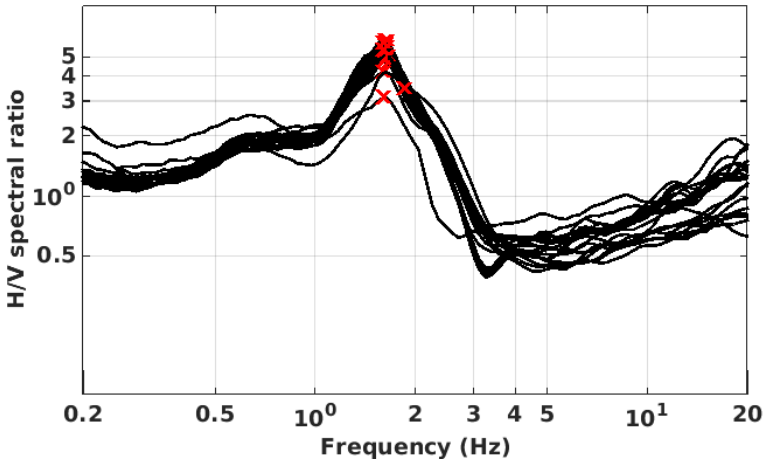

Figure 4: Comparison of H/V spectral ratios (time-frequency analysis code V. Poggi) between the different points of the arrays.

Moreover, all the methods to compute H/V ratios are compared at point WIK000 in Fig. 7, in which the classical methods were divided by $\sqrt{2}$ to correct for the Love waves contribution (Fäh et al., 2001). The 3C FK analysis (Capon method) matches with the H/V analysis but shows the singularity at the trough that is smoothed out by the H/V ratios. The WaveDec results show even more clearly this singularity, corresponding to a change in the sign of the ellipticity angle. In terms of amplitude, all methods match well,

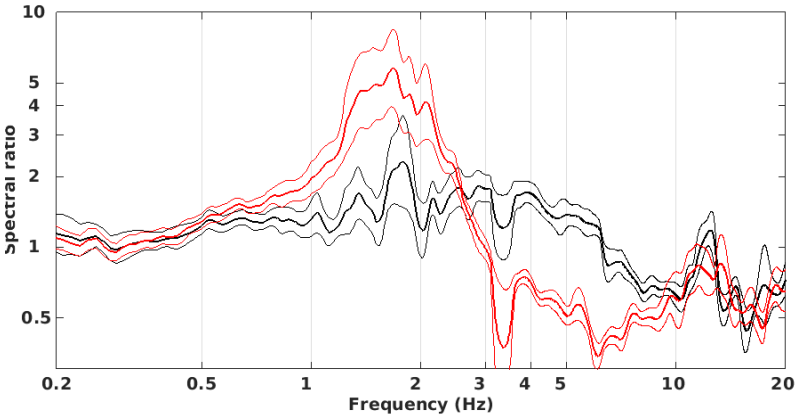

Figure 5: Comparison of H/V spectral ratios at stations XWIL1 (black curve) and XWIL2 (red curve) computed over one week of recording. XWIL2 was located in the school building while XWIL1 was located 800 m North.

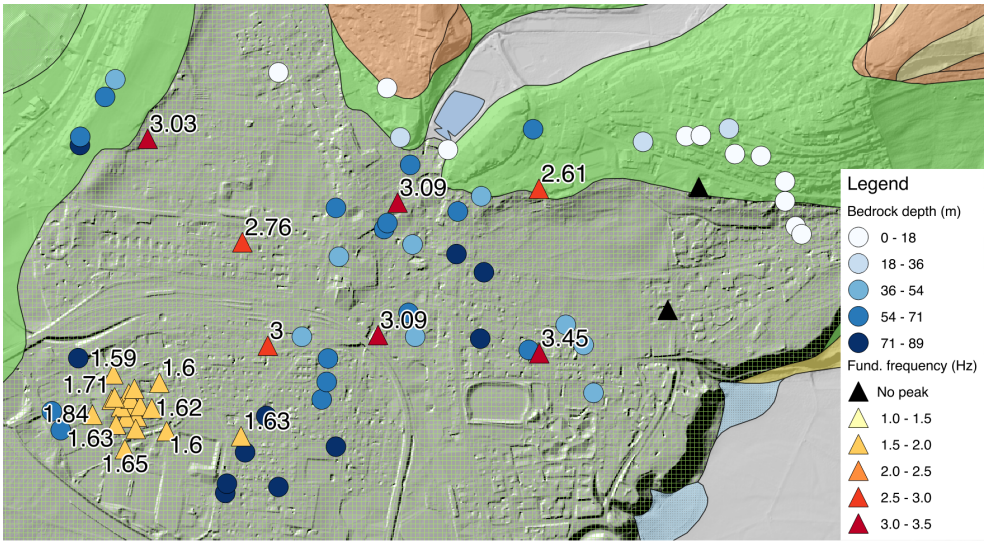

Figure 6: Maps of the identified peaks in the H/V ratios (frequency values in Hz) superimposed on the simplified geological map of the area (see Fig. 2 for the legend).

although the TFA method of V. Poggi, together with the array methods, shows a lower amplitude above the fundamental peak, increasing above the trough. It indicates, first of all that the TFA method of V. Poggi successfully removed the Love wave contribution, and second that this contribution is higher than half of the energy above the fundamental peak at this site, increasing again above the trough.

The fundamental peak at the SWIK station is therefore at 1.62 Hz, with a peak amplitude around 5.

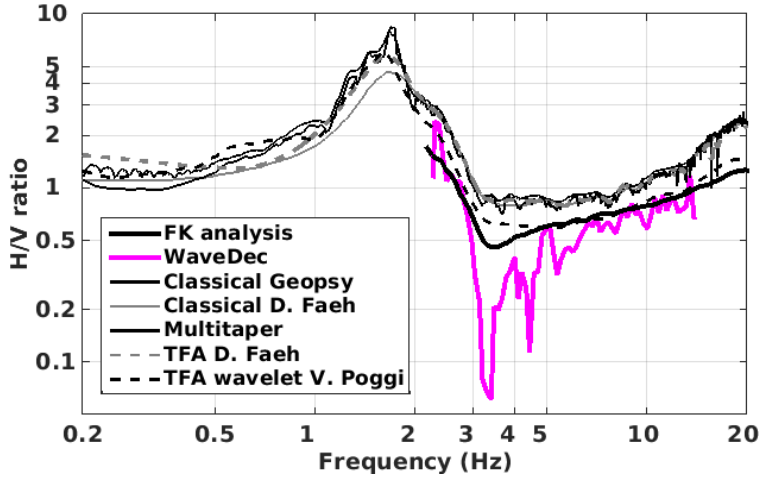

Figure 7: H/V spectral ratios for point WIK000 using the different codes. Classical methods were divided by $\sqrt{2}$.

3.2.2 Polarization analysis

Polarization analysis on the array data was performed to check for 2D resonance using the method of Burjánek et al. (2010). The wavefield shows an elliptic motion in the horizontal direction and polarized in the North-South axis at the fundamental frequency of resonance for all points of the array (Fig. 8). This direction, perpendicular to the highway that is probably the largest contributor of ambient vibrations in the area, is also noticed as the preferred direction in the analysis of surface waves up to 4 Hz. Therefore, the observed polarization could be due to this source and not to a 2D behavior that seems unrealistic considering the valley configuration.

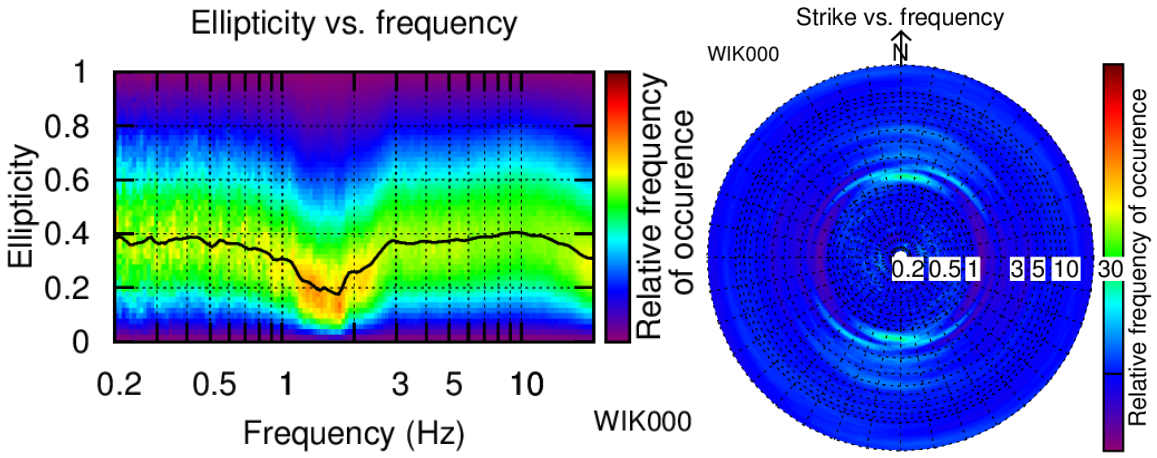

Figure 8: Polarization analysis at point WIK000. Left: Ellipticity (A trough in the ellipticity corresponds to polarized motion). Right: Strike of the polarization.

3.3 3-component high-resolution FK

The results of the 3-component high-resolution FK analysis (Poggi and Fäh, 2010) for the merged results of both configurations are shown in Fig. 9. They are particularly good, this dataset could be used as benchmark to test new methods in the future. The fundamental mode of Rayleigh waves is clearly determined from this analysis in the vertical component between 2.5 and 21 Hz (resolution limit: 2.65 Hz). In the radial component, below 4.5 Hz, the retrieved dispersion deviates from the one obtained with the vertical component. This is likely a problem in the analysis and should be investigated further. From the radial component, higher modes can however be seen. They are picked here but not used in the following. The Love wave fundamental mode can be picked between 1.8 and 6.2 Hz (resolution limit: 2 Hz). Above this frequency, a mode jump is apparent and the fundamental mode, probably dropping to lower velocities, does not have energy anymore. An alternative interpretation with the fundamental mode continuing at higher frequency was tested and discarded during the inversion phase. The first higher mode, though less clear, is picked from 4.6 to 16.3 Hz.
The ellipticity curve determined with the 3-component HRFK analysis is discussed in the H/V analysis.

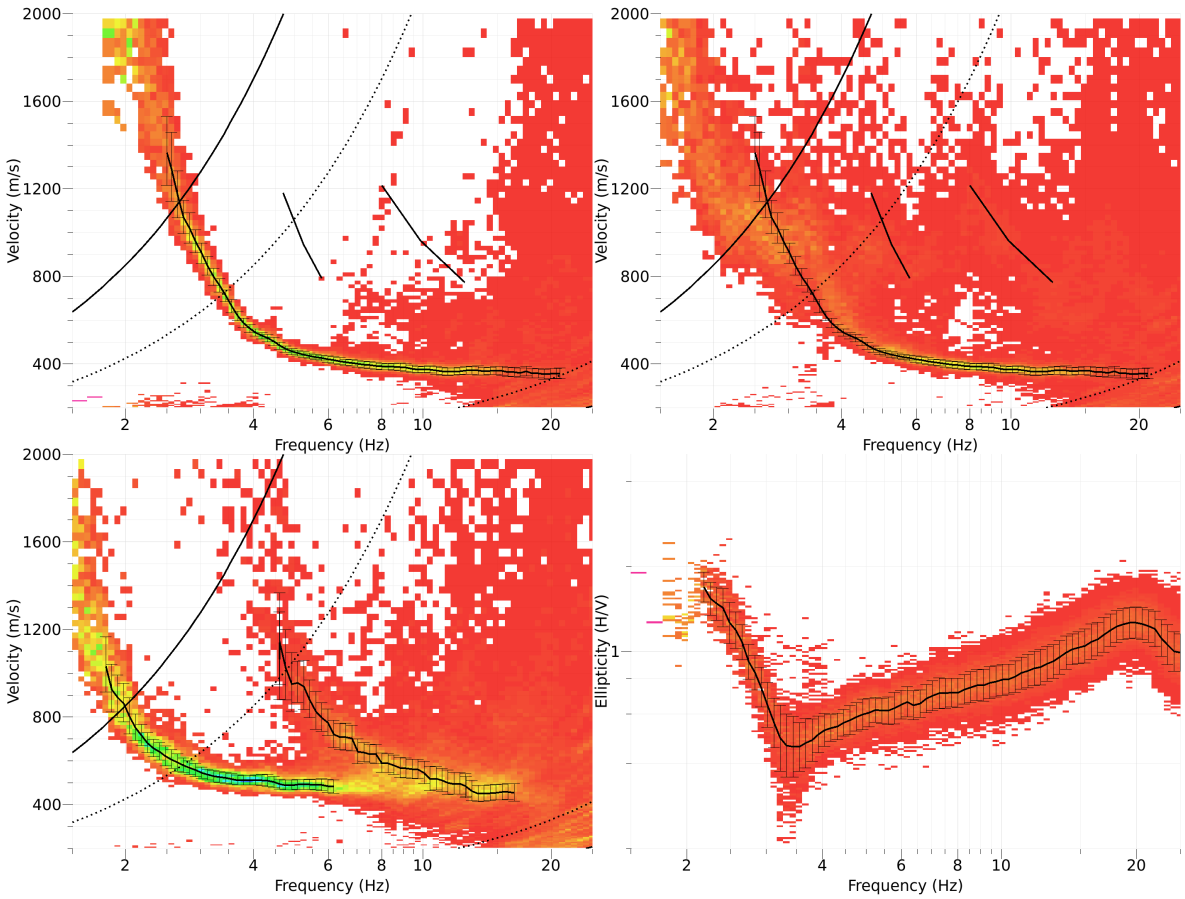

Figure 9: Dispersion curves obtained from the 3C HRFK analyses. Top row: Vertical and radial component; bottom row: transverse component and ellipticity.

3.4 Wavedec

WaveDec (Maranò et al., 2012) has also been used to process the array data WIK2. This technique estimates the properties of multiple waves simultaneously with a maximum likelihood approach in the time domain. It was applied assuming the presence of 3 waves.
The fundamental Love and Rayleigh waves dispersion curves, as well as the first higher Love mode, could be picked (Fig. 10) and are compared to the FK analysis in section 3.5. The ellipticity of Rayleigh waves (Fig. 11) is clear and shows a change in the sense of rotation at about 3.4 Hz (trough). The comparison with other proxys for the ellipticity curve is successfully performed in Fig. 7.

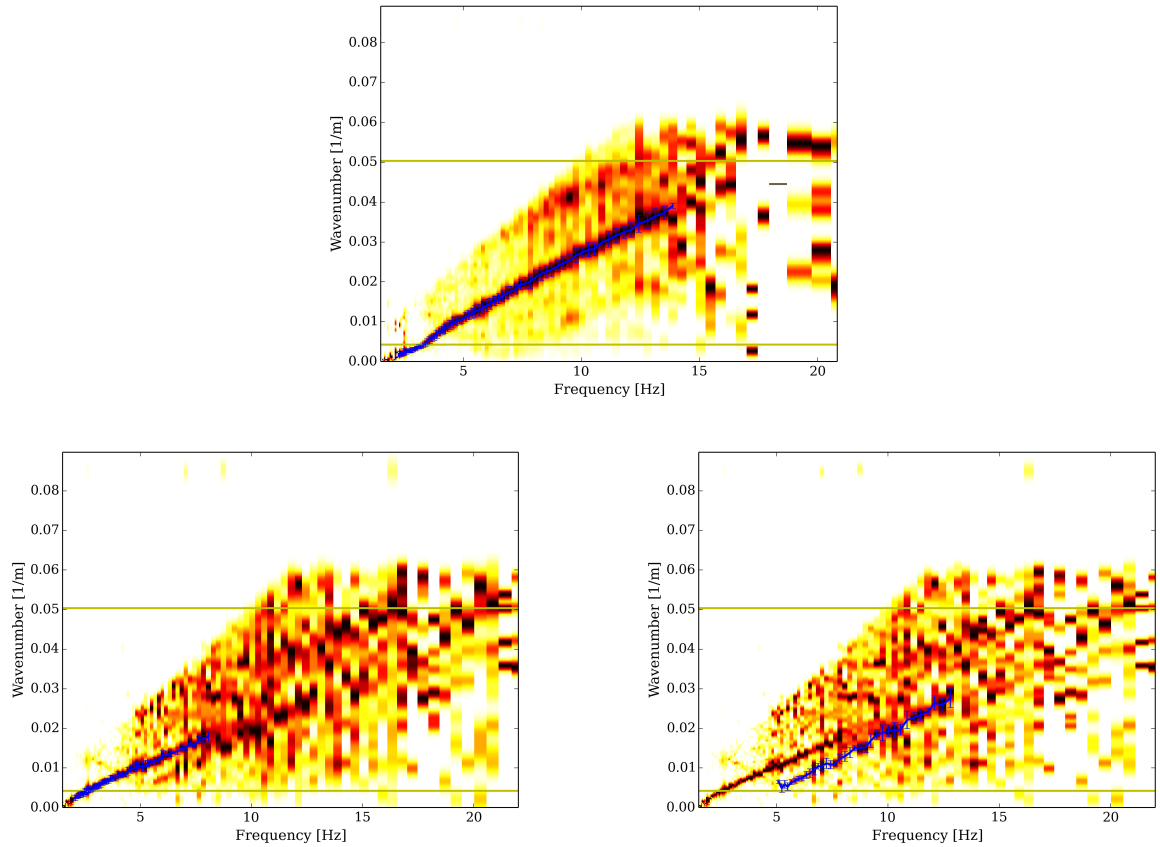

Figure 10: Rayleigh (top) and Love (bottom) waves dispersion curves obtained with the WaveDec technique (Maranò et al., 2012). Picked fundamental (bottom left) and first higher (bottom right) modes of Love waves are shown. The yellow lines indicate the theoretical array resolution limits.

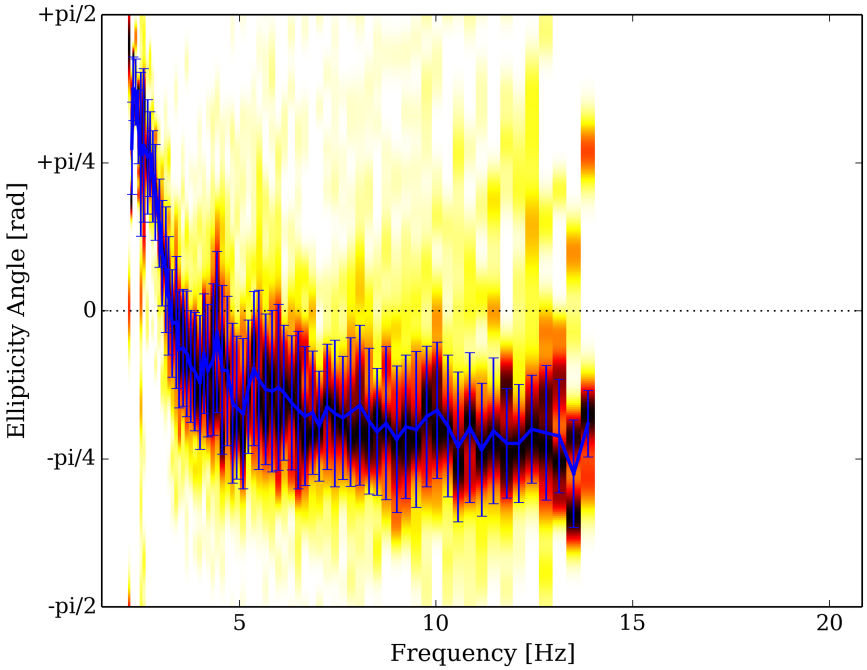

Figure 11: Rayleigh waves ellipticity curve obtained with the WaveDec technique (Maranò et al., 2012).

3.5 Interpretation

Fig. 12 gives an overview of the dispersion curves determined with the different methods. They perfectly agree, though the results from WaveDec are less smooth. A difference can be noted at low frequencies for Rayleigh waves, where WaveDec seems to show an inflexion of the curve not present in the FK results. The finally selected curves are the 3CFK curves, the fundamental mode of Love waves was extended at higher frequency with the WaveDec results and the lower frequency of Rayleigh waves from WaveDec was preferred.

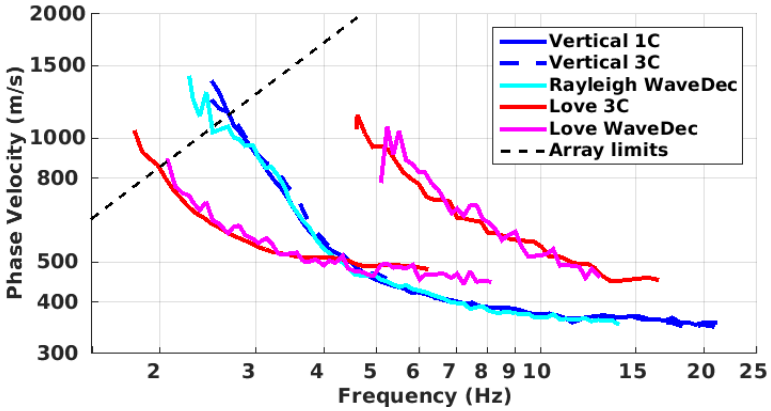

Figure 12: Picked dispersion curves from 3C HRFK analysis and the WaveDec method.

3.6 Data inversion

The inversion of the surface waves properties into 1D velocity profiles was performed using the Improved Neighborhood Algorithm (NA) (Wathelet, 2008) implemented in the Dinver software.

3.6.1 Misfit function

The misfit function is based on the Rayleigh and Love fundamental modes dispersion curves, the Love first higher mode dispersion curve and ellipticity curve based on the WaveDec computation with a weight of 0.2. Moreover, the fundamental resonance frequency at 1.62 Hz was used with a weight of 0.05. However, another value (1.8 Hz) of the fundamental frequency was also tested based on the observation from the empirical spectral modelling (Edwards et al., 2013). In both cases, all curves were resampled using 50 points between 1 and 25 Hz in log scale. No uncertainty was considered in the misfit function (all points with the same weight).

3.6.2 Parametrization of the model space

To parametrize the model space, two assumptions were tested: increasing velocity with depth and the possibility of having a velocity inversion close to the surface. The velocity in the upper part was limited to 600 m/s to avoid unrealistic velocities due to the allowed velocity inversion. The Poisson ratio was inverted in the range 0.2-0.47 (possible presence of water) in the first 20 m and 0.2-0.4 below (no water). The density was assumed to be 2000 kg/m^3 in the sediments and 2500 kg/m^3 in the bedrock. The velocity in the bedrock was limited to 2000 m/s (molasse rock). Inversions with free layer depths as well as fixed layer depths were performed. 3 layers over a half space are enough to explain the targets (dispersion and ellipticity), but more layers are used to smooth the obtained results and better explore the parameter space. 5 independent runs of 5 different parametrization schemes (5 and 6 layers over a half space and 12, 13 and 14 layers with fixed depth) for both assumptions (with and without velocity inversion) and 2 different misfit functions (2 different f_0 values) were performed, i.e. a total of 100 runs.

3.6.3 Results

Examples of retrieved ground profiles for these different assumptions are presented in Fig. 13 and Fig. 15. When comparing to the target curves (Fig. 14 and Fig. 16), dispersion and ellipticity curves are well reproduced. The velocity inversion is not improving dramatically the fit (10% improvement in the misfit) but seems somehow constrained. As a comparison, the free layer depth models have a 10-20% better misfit than the fixed layer depth models. The differences are slight shifts in the Love wave dispersion curves. It allows us to reproduce the ellipticity peak at 20 Hz. It could be due to fluvial sediments sitting over lake sediments: this cannot be excluded by the boreholes, but they do not provide clear evidences.
When the ellipticity fundamental peak is set to 1.8 Hz that is the observed frequency peak in the amplification function from Empirical Spectral Modelling (Edwards et al., 2013), identical misfit values are found. However, the finally retrieved ellipticity fundamental peak remains at 1.6 Hz. The retrieved models with this higher f_0 are slightly shallower (about 10 m) and therefore match better the bedrock depth retrieved from boreholes.

They also force the bedrock depth to realistic values (about 1600 m/s) while the original result leaves this value unconstrained.
For further elaborations, the best models of these 100 runs were selected and used (see section 4.1).

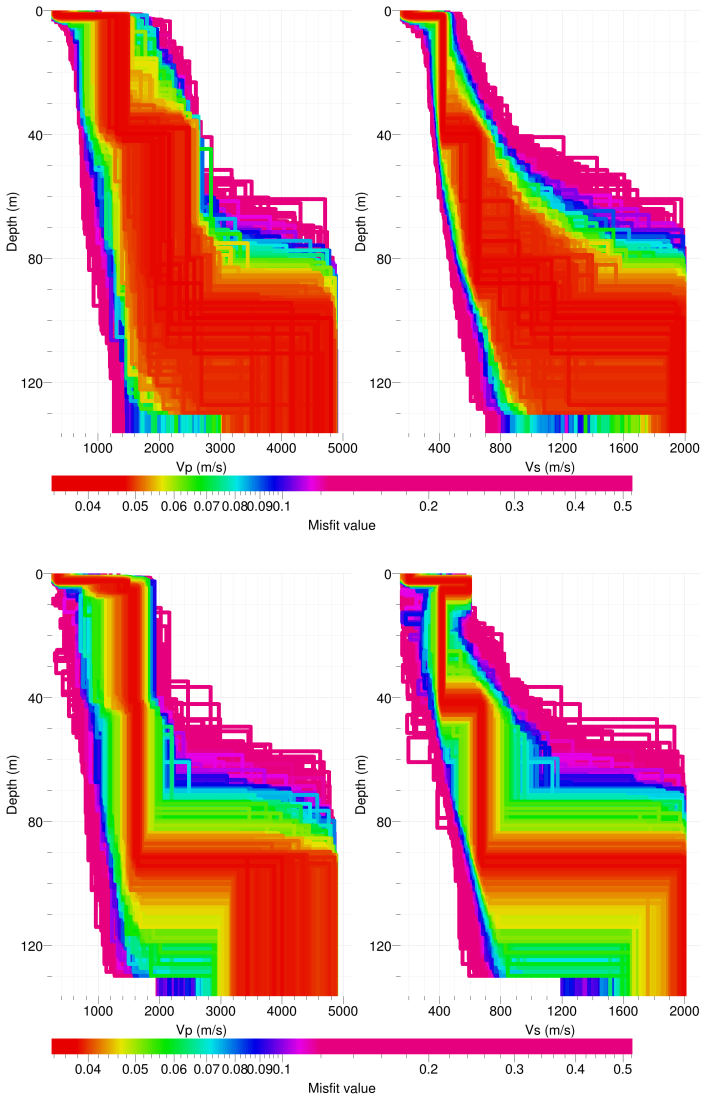

Figure 13: Inverted ground profiles at SWIK in terms of V_p and V_s without (top) and with (bottom) velocity inversion using the free layer depth strategy.

4 Interpretation of the velocity profiles

4.1 Velocity profiles

Excluding the first meter, the profiles all show 90 to 100 m of sediments with velocities from 400 to 750 m/s. A clear contrast within the sediments is present at 40 m depth and is also noticed in the boreholes. A possible zone of higher velocities ranges from 1 to 6 m

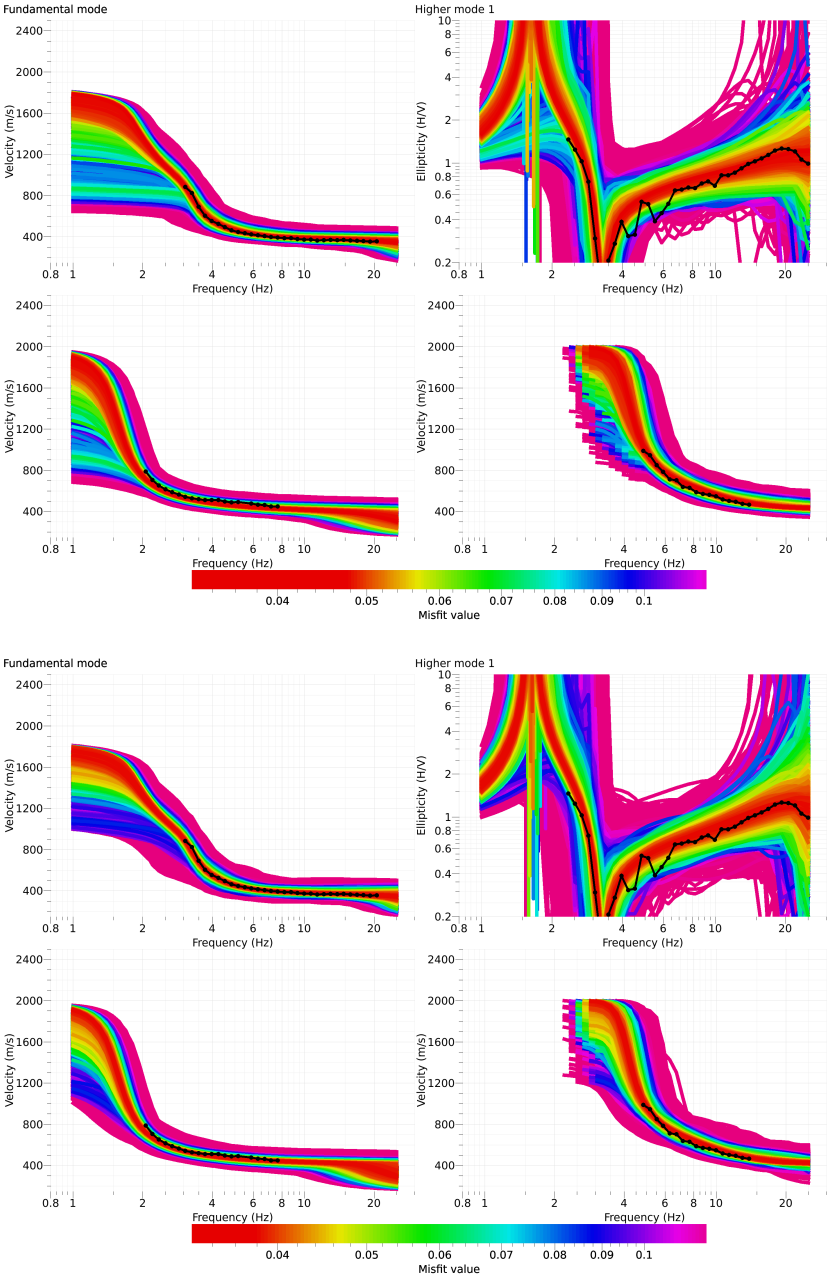

Figure 14: Comparison between inverted models and measured Rayleigh (top row: dispersion and ellipticity) and Love (bottom row: left fundamental and right first higher modes) waves at site SWIK without velocity inversion (top figures) and with velocity inversion (bottom figures).

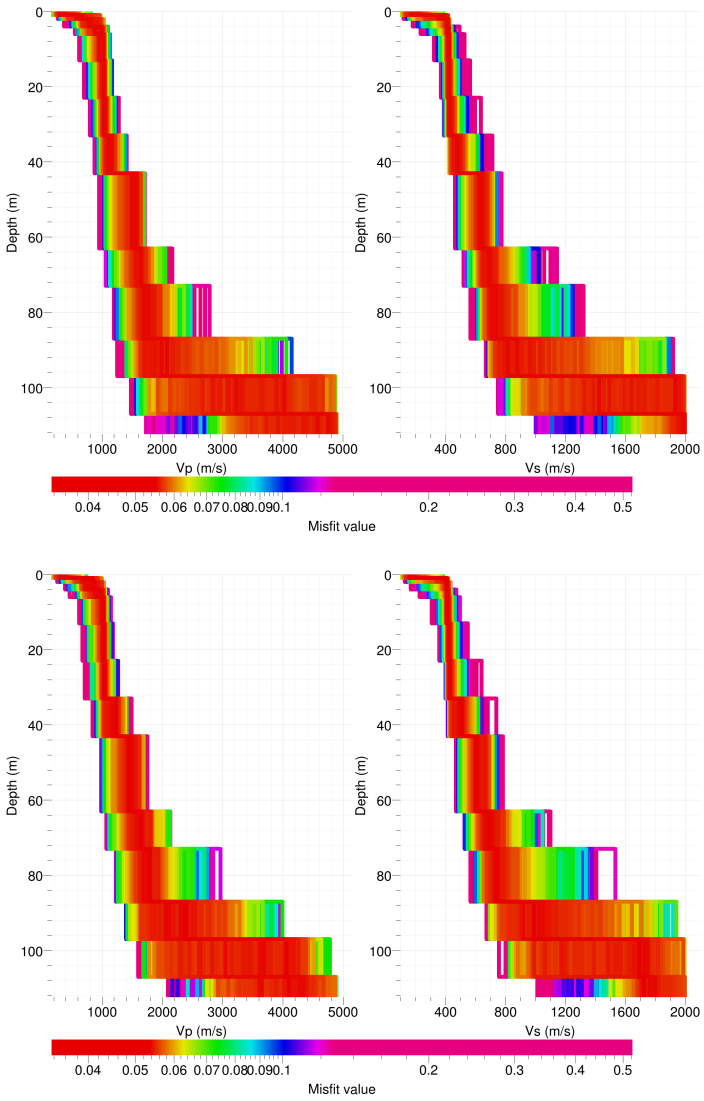

Figure 15: Inverted ground profiles at SWIK in terms of V_p and V_s for a fundamental frequency as observed in the H/V ratios (1.6 Hz, top) and as observed in the ESM function (1.8 Hz, bottom) without velocity inversion and using the fixed layer depth strategy.

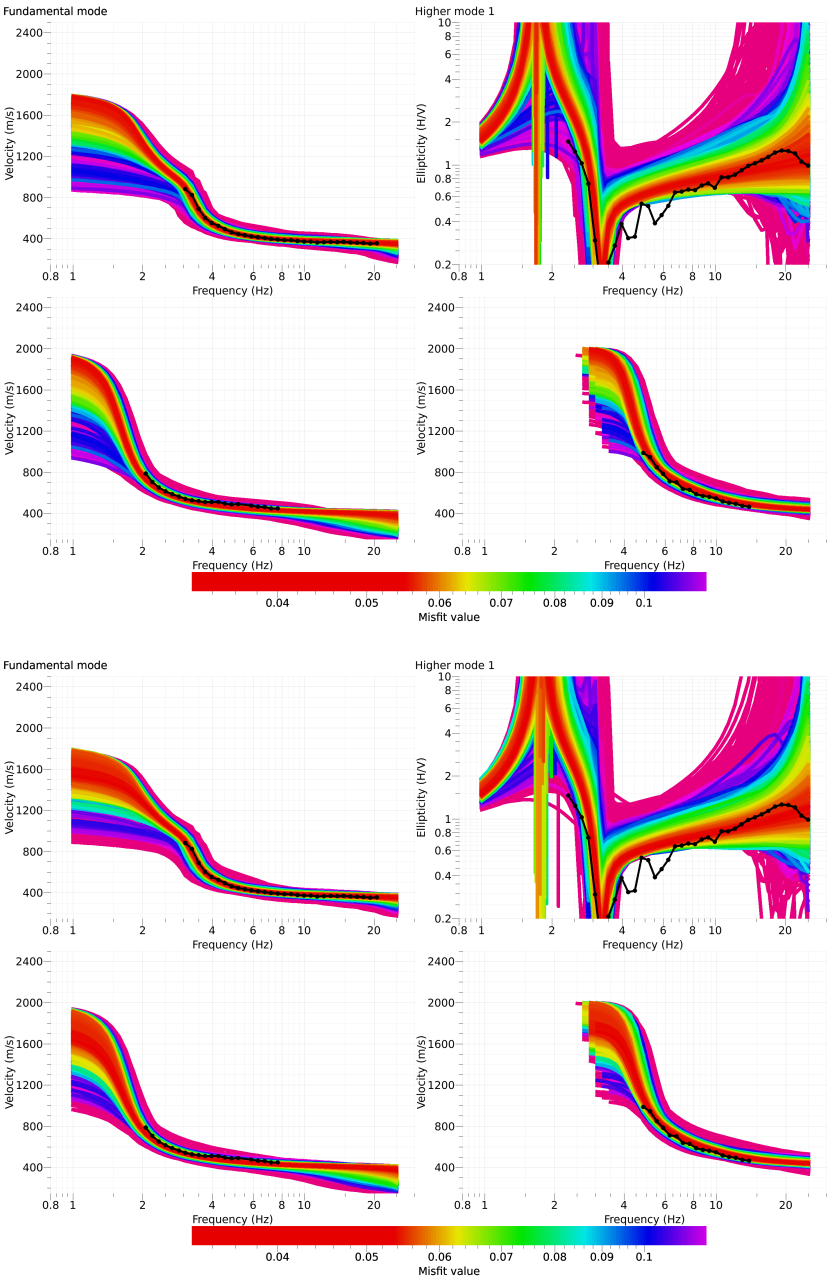

Figure 16: Comparison between inverted models and measured Rayleigh (top row: dispersion and ellipticity) and Love (bottom row: left fundamental and right first higher modes) waves at site SWIK for a fundamental frequency as observed in the H/V ratios (1.6 Hz, top) and as observed in the ESM function (1.8 Hz, bottom) without velocity inversion and using the fixed layer depth strategy.

depth. The velocity contrast is strong with the underlaying rock that is found to be at 1600 m/s if f_0 is set to 1.8 Hz, with higher values in the other cases.

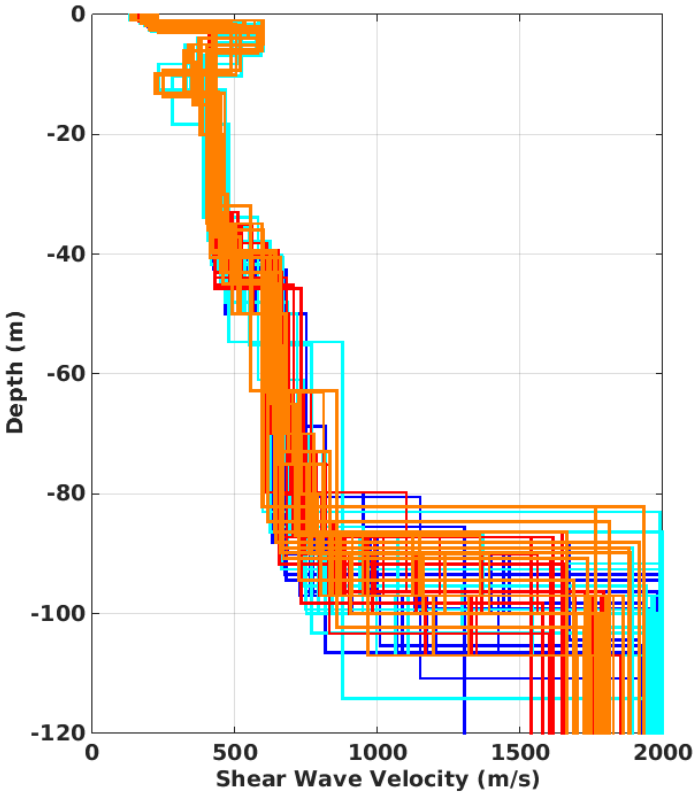

Figure 17: Shear-wave velocity profiles of the 100 selected models. The bluish colors relate to the inversions with f_0=1.6 Hz with (cyan) and without (blue) velocity inversion and the reddish colors to the inversions with f_0=1.8 Hz with (orange) and without (red) velocity inversion

The distribution of the travel time average velocities at different depths was computed from the selected models. $V_{s,30}$ is found to be 397 m/s, corresponding to ground type B in the Eurocode 8 (CEN, 2004) and C in the SIA261 (SIA, 2014).

4.2 Quarter-wavelength representation

The quarter-wavelength velocity approach (Joyner et al., 1981) provides, for a given frequency, the average velocity at a depth corresponding to 1/4 of the wavelength of interest. It is useful to identify the frequency limits of the experimental data (minimum frequency in dispersion curves at 2 Hz and fundamental frequency of resonance at 1.6 Hz). The results using this proxy show that the dispersion curves constrain the profiles down to 50 m and the fundamental frequency to 75 m (Fig. 18). Moreover, the quarter wavelength impedance-contrast introduced by Poggi et al. (2012a) is also displayed in the figure. It corresponds to the ratio between two quarter-wavelength average velocities, respectively from the top and the bottom part of the velocity profile, at a given frequency (Poggi et al., 2012a). It shows a trough (inverse shows a peak) at the resonance frequency.

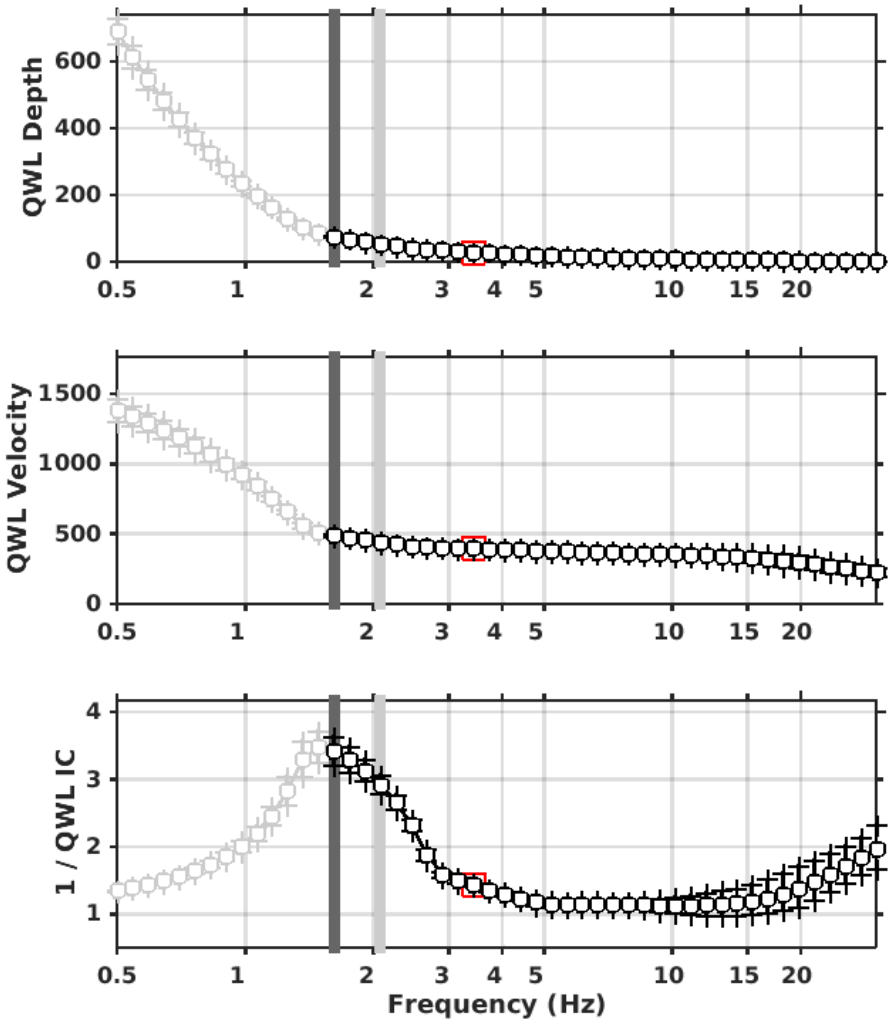

Figure 18: Quarter wavelength representation of the velocity profile for the selected velocity profiles (top: depth, center: velocity, bottom: inverse of the impedance contrast). The black curves are constrained by the dispersion curves, the light grey curves are not constrained by the data. The red square corresponds to V_{S30}.

4.3 SH transfer function

The theoretical SH-wave transfer function for vertical propagation (Roesset, 1970) is computed from the selected profiles. It is corrected with respect to the Swiss Reference Rock model (Poggi et al., 2011) following Edwards et al. (2013). It shows a large peak at the fundamental frequency of resonance reaching an amplification of 5 and further peaks at its harmonics (Fig. 19). It is compared to the amplification function obtained by empirical spectral modelling (ESM) (Edwards et al., 2013; Michel et al., 2014, 2016). Although the empirical amplification for station SWIK is only based on few events so far, the theoretical SH transfer function of the retrieved profiles matches well this observed amplification function (Fig. 19). The peak frequency is slightly shifted to 1.8 Hz as already mentioned and the third peak is also slightly shifted but towards lower frequency (6 Hz instead of 7 Hz from the models). The low velocity zone is not changing the computed function in the frequency range where observation is available. The profiles with a f_0 of 1.8 Hz also do not improve the fit in the peak position compared to the ESM.

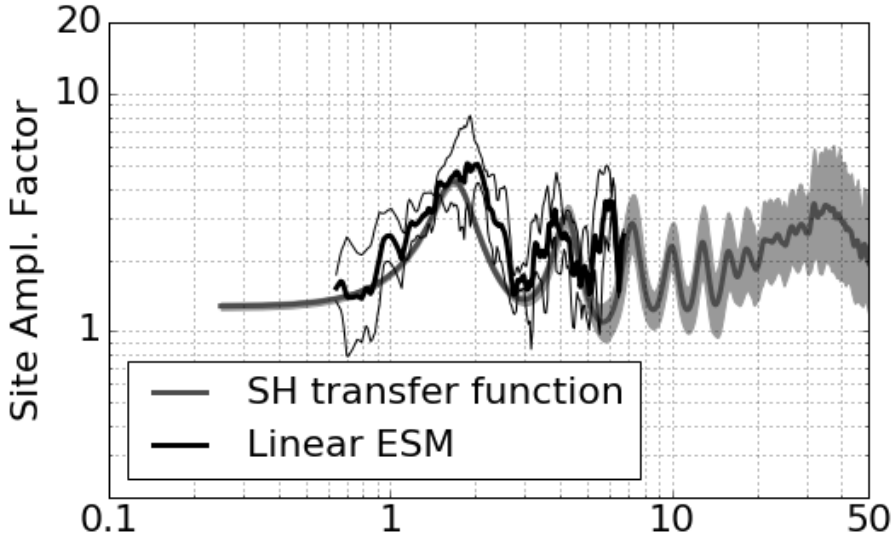

Figure 19: Comparison between the modeled SH transfer function for the selected velocity profiles and the empirical amplification (ESM) measured at station SWIK (with standard deviation).

5 Conclusions

The passive measurements presented in this study were successful in deriving a velocity model for the site SWIK. The site is perfectly 1D and could be used as benchmark for future studies. The profiles show 90 m of alluvial and lacustrine sediments with velocities from 400 to 750 m/s. A clear contrast within the sediments is present at 40 m depth. A possible zone of higher velocities ranges from 1 to 6 m depth without definitive justification. The velocity contrast is strong with the underlaying Upper Freshwater Molasse (OSM) that is found to be at 1600 m/s.
$V_{s,30}$ is 397 m/s and the site corresponds to ground type B in the Eurocode 8 (CEN, 2004) and type C in the SIA261 (SIA, 2014). The theoretical 1D SH transfer function computed

from the inverted profiles shows a large peak at the fundamental frequency at 1.6 Hz reaching an amplification of a factor of 5. This situation is however representative only for the zone around the school area and not for the entire city where higher resonance frequencies and lower velocity contrasts were observed from the H/V measurements.

Acknowledgements

The authors thank David Farsky and Simon Rouwendaal for their help with the array measurements.

References

Burjánek, J., Gassner-Stamm, G., Poggi, V., Moore, J. R., and Fäh, D. (2010). Ambient vibration analysis of an unstable mountain slope. *Geophysical Journal International*, 180(2):820–828.

CEN (2004). *Eurocode 8: Design of structures for earthquake resistance - Part 1: General rules, seismic actions and rules for buildings*. European Committee for Standardization, en 1998-1: edition.

Edwards, B., Michel, C., Poggi, V., and Fäh, D. (2013). Determination of Site Amplification from Regional Seismicity : Application to the Swiss National Seismic Networks. *Seismological Research Letters*, 84(4).

Fäh, D., Kind, F., and Giardini, D. (2001). A theoretical investigation of average H/V ratios. *Geophysical Journal International*, 145(2):535–549.

Joyner, W. B., Warrick, R. E., and Fumal, T. E. (1981). The effect of Quaternary alluvium on strong ground motion in the Coyote Lake, California, earthquake of 1979. *Bulletin of the Seismological Society of America*, 71(4):1333–1349.

Maranò, S., Reller, C., Loeliger, H. A., and Fäh, D. (2012). Seismic waves estimation and wavefield decomposition: Application to ambient vibrations. *Geophysical Journal International*, 191(1):175–188.

Michel, C., Edwards, B., Poggi, V., Burjánek, J., Roten, D., Cauzzi, C., and Fäh, D. (2014). Assessment of Site Effects in Alpine Regions through Systematic Site Characterization of Seismic Stations. *Bulletin of the Seismological Society of America*, 104(6):2809–2826.

Michel, C., Fäh, D., Edwards, B., and Cauzzi, C. (2016). Site amplification at the city scale in Basel (Switzerland) from geophysical site characterization and spectral modelling of recorded earthquakes. *Physics and Chemistry of the Earth, Parts A/B/C*.

Poggi, V., Edwards, B., and Fäh, D. (2011). Derivation of a Reference Shear-Wave Velocity Model from Empirical Site Amplification. *Bulletin of the Seismological Society of America*, 101(1):258–274.

Poggi, V., Edwards, B., and Fäh, D. (2012a). Characterizing the Vertical-to-Horizontal Ratio of Ground Motion at Soft-Sediment Sites. *Bulletin of the Seismological Society of America*, 102(6):2741–2756.

Poggi, V. and Fäh, D. (2010). Estimating Rayleigh wave particle motion from three-component array analysis of ambient vibrations. *Geophysical Journal International*, 180(1):251–267.

Poggi, V., Fäh, D., Burjánek, J., and Giardini, D. (2012b). The use of Rayleigh-wave ellipticity for site-specific hazard assessment and microzonation: application to the city of Lucerne, Switzerland. *Geophysical Journal International*, 188(3):1154–1172.

Roesset, J. (1970). Fundamentals of soil amplification. In Hansen, R. J., editor, *Seismic Design for Nuclear Power Plants*, pages 183–244. M.I.T. Press, Cambridge, Mass.

SIA (2014). *SIA 261 Einwirkungen auf Tragwerke*. Société suisse des ingénieurs et des architectes, Zurich, Switzerland.

Wathelet, M. (2008). An improved neighborhood algorithm: Parameter conditions and dynamic scaling. *Geophysical Research Letters*, 35(9):1–5.